

Renewable Energy Research and Applications (RERA)



Vol. 6, No. 2, 2025, 179-190

DOI: 10.22044/rera,2025.16894.1477

Robust Static Quadratic Optimization for Fast Active and Reactive Power Control in Grid-Tied PV-Fuel Cell Hybrid Systems

Muftah. Magdi G¹, Salem. Mohamed^{1*}, M. Swadi², Kh. Ben Hamad³, M. Kamarol¹

School of Electrical and Electronic Engineering, Universiti Sains Malaysia, Nibong Tebal, 14300, Penang, Malaysia.
 Department of Electrical Engineering, College of Engineering, University of Baghdad, Baghdad 10001, Iraq.
 Department of Electrical and Electronic Engineering, Fezzan University, Fezzan, Libya.

Received Date 27 September 2025; Revised Date 27 October 2025; Accepted Date 04 November 2025
**Corresponding author: salemm@usm.my (Salem. Mohamed)

Abstract

This paper proposes a new modified P–Q control scheme with a simple design using Static Quadratic Optimization (SQO) concept for a grid-connected hybrid system of photovoltaic (PV) and Fuel Cell (FC) sources. Contrary to traditional design practices involving voltage-oriented control (VOC) employing proportional-integral (PI) controllers or existing predictive strategies involving quadratic optimization by iterative computation, this proposed design of SQO directly computes an analytical expression of dq-axis current references as the optimal solution of a static-quadratic cost minimization problem. The proposed design enables optimal real and reactive power control simultaneously in a single step. The design of an efficient voltage-oriented current controller effectively utilizes measured values of grid current and voltage, as well as reference powers, which allows optimal bidirectional reactive controlled supply or absorption of reactive powers according to grid needs. The simulation of the grid-connected system has been performed in a MATLAB/Simulink environment. The simulation outcome verified the proposed P-Q voltage-oriented current controller design with a power factor of 0.998, phase displacement of 0.12°, total harmonic distortion (THD) levels of 1.2% for current and 0.39% for voltage, strictly within the IEEE-519 standards.

Keywords: *Grid-tied inverter, photovoltaic- fuel cell hybrid system, active and reactive power control, power factor correction, smart grid integration.*

1. Introduction

The increasing world demand for renewable and been propelling energy has technological innovation in renewable energy technology. Of them, the photovoltaic (PV) and fuel cell (FC) systems have been of great interest because they have complementary features—PV offers clean but intermittent power, whereas fuel cells offer stable but dispatchable power output [1], [3]. Combined, PV-FC hybrid systems have a potential solution for providing a constant and stable power supply to the utility grid, especially for changing solar irradiation or dynamic loads [1]. However, PV-FC systems integration into the grid is not problem-free. The primary operation challenge among them is to control active and reactive power to provide voltage stability, power quality, and grid code conformance [2], [5], [6]. The grid-connected renewables' inverters were single-minded about injecting active power only until the smart grid age, but now the decentralized energy systems have to provide ancillary services

compensation. reactive such dvnamic frequency regulation, and voltage buck-up [4], [7], [14]. Some active/reactive power control techniques for PV-based systems were discussed. For example, intelligent, predictive, etc., type control techniques were discussed to optimize the power exchange between the grid and the PV sources by [4] and [6]. Some other studies explored grid voltage regulation using dynamic reactive power regulation, grid synchronization [5], [14], [15], etc. Surprisingly, [10] and [11] discussed some advanced voltage regulation techniques by the multilevel inverters, such as active filtering by active power filters to improve the systems' stability.

Because of the high-dynamic response and controllable output, the fuel cells were thus suggested to assist reactive power compensation and grid fault ride-through characteristics, particularly with local inductive loads [3], [17]. For the hybrid systems, the FC module supports

the generation by the PV throughout low irradiation levels with the operation of voltage assist along with reactive power regulation [1], [3], [18].

It has been emphasized by recent studies on the decoupled active and reactive power management for enabling the renewable sources to respond individually to the real and reactive power demands [7], [19], [20]. The concept has been further extended in [24] based on Model Predictive Control (MPC) for enhanced dynamics performance for three-phase systems. Besides, hybrid energy systems based on Battery Energy Storage Systems (BESS) also proved viable for hosting the constraints on the inverter currents and active/reactive power scheduling [12].

To realize longer grid support features, [9] and [13] suggested smart MPPT schemes and IoTbased schemes for the PV stations to realize adaptive reactive power reserve and power flow controllability. Single-stage, transformerless, and bidirectional power controllability were also explored to realize minimum energy loss to the absolute minimum [21], [16], [22]. Nevertheless, it is challenging to integrate the PV-FC hybrid with optimal active/reactive power coordination, especially with dynamic, unbalanced conditions [17], [8]. The research cited in [23]-[27] also studies the control of active and reactive grid systems using either open-loop P-Q techniques or closed-loop systems based on artificial neural networks or field-oriented control techniques. The methods, however, cannot attain a state of zero error when controlling the P-Q parameters. Recent advances have been achieved in the hybrid PV-FC control system and reactive power compensation. For hybrid PV-FC, [28] reported the Tapped Delay Control-LMS (TDC-LMS) algorithm for smart grid fuel cells. For PV-FC battery charging of electric vehicles (EVs), [29] designed an Adaptive Neural-Fuzzy Inference System-based Maximum Power Point Tracking (ANFIS-MPPT) method. For gridconnected renewables, [30] optimized STATCOM controls. These developments reinforce the existing literature, indicating the continued importance of this proposed SQO technique.

Despite the progress achieved by VOC-, MPC-, and AI-based controllers, most existing strategies still face challenges such as dependence on iterative tuning, limited robustness under fast dynamic conditions, and increased computational burden due to complex feedback loops. In addition, these methods often exhibit slower transient response and reduced precision in

decoupling active and reactive power, especially under rapid changes in irradiance and load.

For this purpose, the proposed SQO technique will address the problem of iterative regulation by finding the optimal dq current references through an analytic cost function optimization process. This aims to ensure rapid dynamics, robustness, and a higher level of power quality. The main contributions of this paper are

- 1) The paper introduces an SQO method that computes dq-axis current references analytically in a single step, eliminating the need for PI tuning and iterative control.
- 2) The proposed controller enables fast, bidirectional active and reactive power regulation with improved dynamic performance under variable conditions.
- 3) The SQO approach achieves high power quality and near-unity power factor with minimal THD, outperforming VOC, MPC, and ANN-based methods.

The following sections of this paper are organized into six separate parts. Section 2 defines the problem formulation, and section 3 discusses the system modeling. Section 4 states the proposed control policy. Section 5 presents the results achieved, and section 6 includes a discussion on the performance comparison, leading to section 7, which contains the concluding remarks.

2. Problem formulation

This section begins with the system description, then problem identification and ends with the control objective.

2.1. System description

First, the under-consideration grid-connected inverter system is coupled with different energy sources, comprising a total rated capacity of 300 kW, including a photovoltaic (PV) array and a fuel cell unit. The regulation strategy aims to provide harmonized active and reactive power regulation with a near-unity power factor. For this purpose, the regulation is performed in the synchronous dq reference frame using a closedloop feedback structure. The inverter's output currents and voltages are measured and converted through a Phase-Locked Loop (PLL), and the extracted grid angle is suitable for accurate conversion to the dq frame. The active and reactive power are calculated online from the converted quantities and compared against the desired values. Power errors and measured grid voltage components are processed through a quadratic-based power tracker optimization algorithm instead of a conventional PI-based power regulator. This algorithm calculates the optimal d- and q-axis current references by minimizing a weighted power tracking penalty on over-current magnitudes, enabling harmonized tuning of the two current components to simultaneously regulate active and reactive power. The resulting current references are then regulated to generate inverter voltage commands, which are converted back to the three-phase frame and fed to the PWM stage to produce switching commands. This strategy ensures correct and dynamic regulation even under load and grid variations while maintaining a near-unity power factor. This configuration establishes the foundation for identifying the main operational challenges associated with hybrid PV-fuel cell integration, as discussed next.

2.2. Problem Identification

Building upon the described system, the following subsection identifies the key control issues that motivate the development of the proposed approach. In PV array-fuel cell hybrid solar power systems, such as the 300-kW installation presented here, the grid-side inverter should regulate active and reactive power sustainably and at a power factor near unity. PI regulators are popularly used for this but carry inherent drawbacks such as low dynamical response to high-level transients, reduced tracking accuracy under parameter changes, poor control of inherent active-reactive coupling, and high tunability. Such drawbacks become critical in large multisource installations, where operating conditions are often variable. As a mitigation, this work closed-loop, quadratic-based employs a optimization regulation strategy that computes the optimal d- and q-axis current references from power feedbacks available in real time and grid voltage measurements.

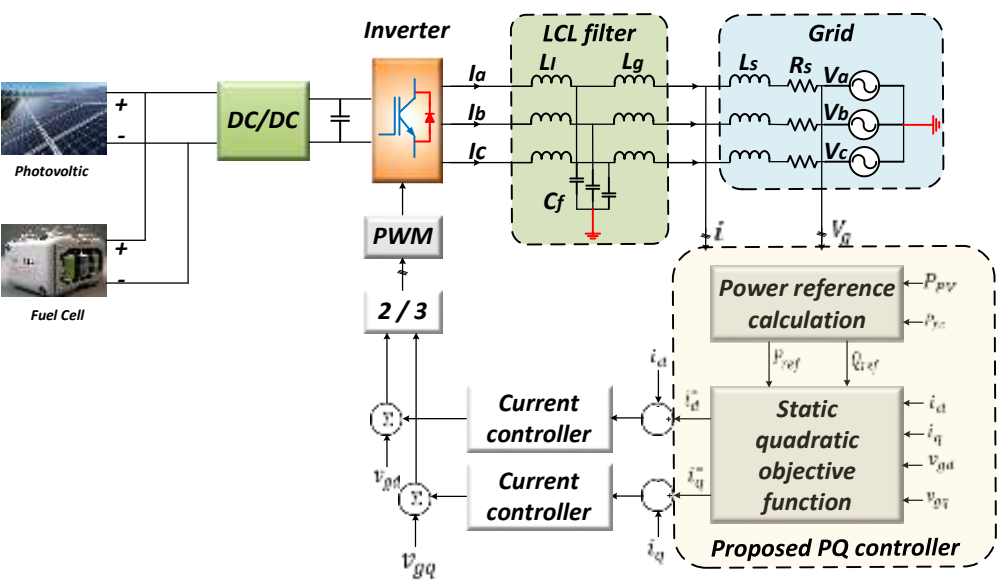


Figure 1. Proposed system.

By defining power regulation as minimizing a quadratic cost problem, the approach auto governances controlling on active—reactive coupling, maintains tracking accuracy, and detests high current magnitude, leading to quicker, tougher, and accurate performance over and above conventional PI-based regulation.

2.3. Control Objective

After defining the control problem, this subsection formalizes the control objectives that the proposed optimization-based approach aims to achieve. Therefore, the initial control objective is to regulate the grid-connected inverter's active and reactive power to track their respective reference

commands while maintaining a power factor close to unity. This requirement can be expressed mathematically as

$$\lim_{t \to \infty} (P(t) - P^*) = 0, \lim_{t \to \infty} (Q(t) - Q^*) = 0$$
 (1)

where P(t) and Q(t) represents the instantaneous active and reactive powers, respectively, P^* , Q^* denote their reference commands. With the additional constraint for a near-unity power factor PF

$$PF = \frac{P}{\sqrt{P^2 + Q^2}} \approx 1 \tag{2}$$

The control law must ensure that both power tracking errors converge to zero while minimizing

the current magnitude $\|\mathbf{i}_{dq}\|$ to reduce the inverter stress.

3. Energy sources modelling

3.1. PV system model

The photovoltaic array is modeled using a single-diode equivalent circuit, as shown in figure 2, which is included in [23, 24], where the output current is determined by the balance of photocurrent, diode current, and shunt leakage current. The key electrical relation is given in (7), and the main PV parameters are listed in table 1.

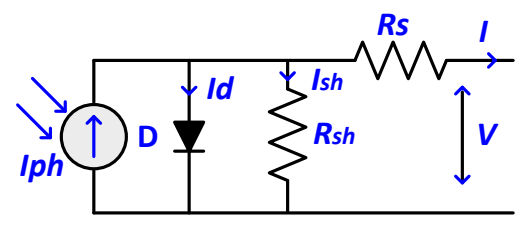


Figure 2. PV cell Equivalent circuit.

The general current-voltage relationship can be expressed as follows:

$$I = I_{ph} - I_d - I_{sh} \tag{3}$$

The photocurrent depends on the solar irradiance and cell temperature.

$$I_{ph} = \frac{G}{G_{STC}} \left(I_{phSTC} + \mu (T - T_{STC}) \right) \tag{4}$$

The diode and shunt currents can be defined as:

$$I_{d} = I_{sat} \left(exp \left(\frac{V + R_{s}I}{nV_{t}} \right) - 1 \right)$$
 (5)

$$I_{sh} = \frac{V + R_s I}{R_{sh}} \tag{6}$$

Combining these yields the complete PV cell equation:

$$I = \frac{G}{G_{STC}} \left(I_{phSTC} + \mu (T - T_{STC}) \right) - I_{sat} \left(exp \left(\frac{V + R_s I}{nV_t} \right) - 1 \right) - \frac{V + R_s I}{R_{sh}}$$

$$(7)$$

Here, G and G_{STC} are the actual and standard irradiance levels, R_s and R_{sh} are the series and shunt resistances, I_{sat} is the diode saturation current, n is the ideality factor, V_t is the thermal voltage, and μ is the temperature current coefficient. The main specifications of the PV system for one module and the entire system are listed in table 1.

Table 1: The specification of the PV system [23].

Parameter	Value and unit
Maximum power	150 kW
Module power	280.2 W
Open circuit voltage (V_{oc})	45.1 V
Short-circuit current (I_{sc})	8.34 A
Maximum voltage (V_{mpp})	35.9 V
Maximum current (I_{mpp})	7.8 A
Cells per module (N _{cell})	72
Parallel strings (N _{PS})	39
Series-connected modules per string	14
Light-generated current (I_{Ph})	8.3516 A
Diode saturation current (I_S)	1.8445e ⁻¹⁰ A
Diode ideality factor (A)	0.99427
Shunt resistance (R_{sh})	362.9175 Ω
Series resistance (R_S)	0.49012 Ω

3.2. Fuel cell modelling

A fuel cell converts the chemical energy of hydrogen and oxygen directly into electrical energy through an electrochemical reaction without combustion. The general configuration and equivalent circuit of the proton exchange membrane (PEM) fuel cell stack are shown in figure 3 [3], [23], [25].

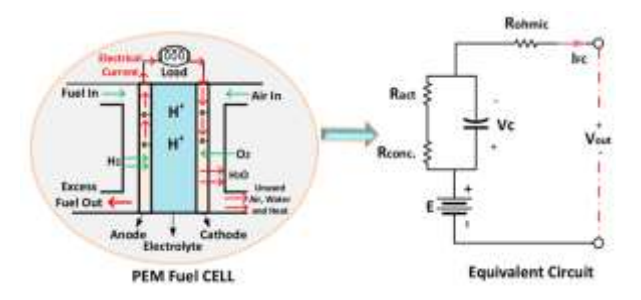


Figure 3. Operational structure and equivalent circuit of a fuel cell.

The output voltage of the fuel cell stack can be written as [23]

$$V_{FC} = N_{Cell} E_{Cell} = E - V_{Act.} - V_{Conc.} - V_{Ohmic}$$
 (8)

where V_{FC} denotes the total stack voltage, E is the open circuit voltage, and $V_{Act.}$, $V_{Conc.}$, and V_{Ohmic} represents the activation, concentration, and ohmic voltage losses, respectively.

Furthermore, the characteristics of the voltagecurrent of the fuel cell stack can be modelled as [25]

$$V_{FC} = E - AT \ln \left(\frac{I_{FC}}{I_{O}}\right) - BT \ln \left(\frac{I_{L} - I_{FC}}{I_{L}}\right) - I_{FC}R_{int} \tag{9}$$

Here, I_{FC} is the output current of the fuel cell stack, I_{O} is the exchange current, I_{L} denotes the limiting current, R_{int} represents the internal resistance, A and B are the activation and concentration coefficients, and T is the absolute

temperature. The parameters for a 150 kW fuelcell system used with the PV system are listed in table 2.

Table 2: The specification of the FC system [23].

Parameter	Value and unit		
Stack temperature (T)	338oK		
Activation area (A)	50.6 cm2		
Membrane thickness (l)	178 μm (Nation 117)		
Hydrogen pressure (P _{H2})	1 atm		
Oxygen pressure (P _{O2})	1 atm		
Dynamic capacitor (C)	3 F		
Membrane contact resistor (R _C)	$0.0003~\Omega$		
Computing coefficient (B)	0.016		
Curve fitting parameter (ζ_1)	-0.948		
Curve fitting parameter (ζ_2)	0.00312		
Curve fitting parameter (ζ_3)	7.6 e ⁻⁵		
Curve fitting parameter (ζ_4)	-1.93e ⁻⁴		
Membrane moisture content (Ψ)	23		
Current density (I _L)	$1500 \mathrm{mA/cm^2}$		
Stack nominal power	150 kW		
Maximum power	162.8 kW		
Efficiency	55 %		
Number of cells	2000		

3.3. Interleaved boost converter design

The interleaved boost converter functions as an interface between both the PV and FC sources and the common DC bus. It reduces current ripples. The structure of this converter is shown in figure 4 [23], [25]. The interleaved boost converter employs multiple phases that switch with the same duty cycle but with phase-shifted signals. This approach minimizes current ripples on both the input and output sides. The interleaved boost converter enhances the converter's efficiency, electromagnetic interference (EMI) isolation, and current distribution.

The output of each phase can be expressed as

$$V_{o} = \frac{V_{in}}{1 - D} \rightarrow D = 1 - \frac{V_{in}}{V_{o}}$$
 (10)

The output and input currents can be calculated as

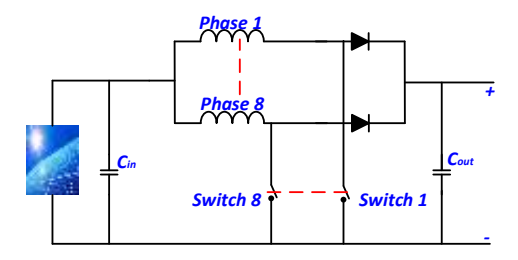


Figure 4. PV system based on an interleaved boost converter.

$$I_{o} = \frac{V_{o}}{R_{L}} \text{ or } \frac{P}{V_{o}}$$

$$I_{in} = \frac{P}{V_{in}}$$
(11)

$$I_{\rm in} = \frac{\bar{P}}{V_{\rm co}} \tag{12}$$

In order to design the inductance and capacitance of the converter during the ON state of switching, these passive elements can be designed based on the following expressions.

$$L \ge \frac{V_{\rm in}D}{\Delta i_L f_s} \tag{13}$$

$$i_{L,pk} \approx \frac{I_{\varphi}}{N} + \frac{\Delta i_L}{2} \tag{14}$$

$$C_o \ge \frac{I_o D}{\Delta V_o f_s} \tag{15}$$

$$C_{\rm in} \ge \frac{I_{\rm in} D}{N\Delta V_{\rm in} f_{\rm s}} \tag{16}$$

The design values for each phase are listed in table 3 depending on the above expressions.

Table 3: The design specification of the interleaved boost converter for PV and FC

Item	Symbol	Value
Phases	N	8 interleaved
Power	P	150 kW per source
Input voltage	V_{in}	500 V
DC-bus voltage	V_o	800 V
Duty ratio	D	0.375
efficiency	η	96%
Per-phase avg input current	$I_{\phi} = \frac{I_{in}}{N}$ $I_{in} = \frac{P}{V_{in}}$	37.5 A
Input current	$I_{in} = {}^{P}/_{V_{in}}$	300 A
Output current	$I_{o} = \frac{\eta P}{V_{o}}$ I_{pk}	180 A
Inductor peak current	I_{pk}	41.3 A
PWM phase shift	360°/ _N	45°
Inductance	L	1.25 m <i>H</i>
Output capacitance	C_o	52.5 μF
Input capacitance	C_{in}	281 μF
Switching frequency per	f_s	20 kHz
phase		

4. Proposal control scheme

Unlike the work in [31], which employs a linear quadratic regulator based on a dynamic statefeedback law derived from the Riccati equation, this paper proposes a static quadratic optimization method formulates the that outer-loop power control active/reactive as static optimization problem in the dq-frame, with instantaneous bus voltage vector G explicitly embedded in the control law, as shown in figure 5. The proposed approach achieves a tunable tradeoff between zero steady state tracking error of active and reactive power control and reduced current stress on the inverter by defining a proper cost function.

As depicted in figure 5, the proposed control scheme is developed within a synchronous reference frame to enable decoupled active and

reactive power regulation. First, the three-phase voltages and currents are expressed as

$$\mathbf{v}_{abc} = \begin{bmatrix} v_a \\ v_b \\ v_c \end{bmatrix}, \mathbf{i}_{abc} = \begin{bmatrix} i_a \\ i_b \\ i_c \end{bmatrix} \tag{17}$$

and transformed into a stationary orthogonal $\alpha\beta$ frame through the Clarke transformation.

$$\begin{bmatrix} v\alpha \\ v\beta \end{bmatrix} = T_{\alpha\beta}v_{abc}, \qquad \begin{bmatrix} i\alpha \\ i\beta \end{bmatrix} = T_{\alpha\beta}i_{abc}$$
 (18)

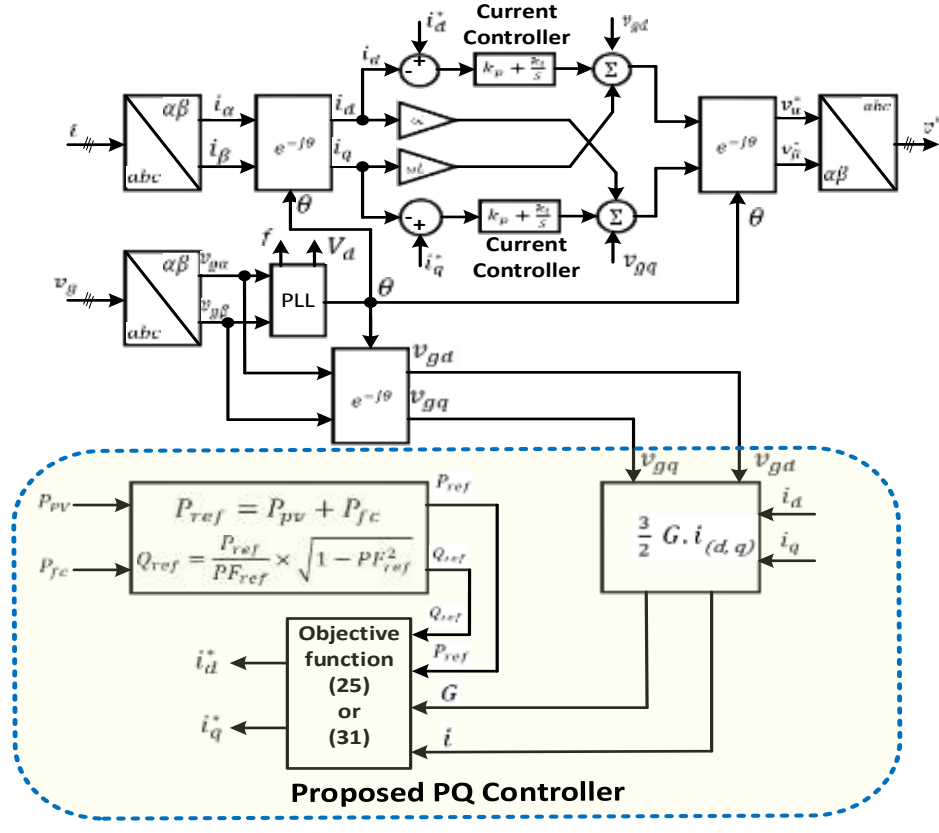


Figure 5. Proposed control scheme.

where

$$[T_{\alpha\beta}] = \sqrt{\frac{2}{3}} \begin{bmatrix} 1 & -\frac{1}{2} & -\frac{1}{2} \\ 0 & \sqrt{\frac{3}{2}} & -\sqrt{\frac{3}{2}} \end{bmatrix}$$
 (19)

Using the grid voltage angle θ obtained from a phase-locked loop (PLL), these quantities are then rotated into the synchronous dq frame via the Park transformation.

$$T_{dq}(\theta) = \begin{bmatrix} \cos(\theta) & \sin(\theta) \\ -\sin(\theta) & \cos(\theta) \end{bmatrix}$$
 (20)

$$\begin{bmatrix} vd \\ vq \end{bmatrix} = T_{dq} \begin{bmatrix} v\alpha \\ v\beta \end{bmatrix}, \text{ and } \begin{bmatrix} id \\ iq \end{bmatrix} = T_{dq} \begin{bmatrix} i\alpha \\ i\beta \end{bmatrix}$$
 (21)

In the dq frame, the instantaneous active and reactive powers are calculated as

$$P = \frac{3}{2} \left(v_{gd} i_{gd} + v_{gq} i_{gq} \right) \tag{22}$$

$$Q = \frac{3}{2} \left(v_{gq} i_{gd} - v_{gd} i_q \right) \tag{23}$$

These can be expressed in a compact form.

$$\begin{bmatrix} P \\ Q \end{bmatrix} = \frac{3}{2} \underbrace{\begin{bmatrix} v_{gd} & v_{gq} \\ -v_{gq} & v_{gd} \end{bmatrix}}_{G} \begin{bmatrix} i_{gd} \\ i_{gq} \end{bmatrix} = \frac{3}{2} \text{ G. i}$$
(24)

while conventional strategies such as PI, ANN, or fuzzy controllers generate the current references (i_q^*, i_q^*) in the outer P-Q loops, the proposed method replaces these with a quadratic optimization-based controller. The objective is to minimize the tracking error of active and reactive power while penalizing excessive current magnitude, formulated as

$$J(i) = (G. i - P^*)^{T} Q_{\omega}(G. i - P^*) + i^{T} R_{\omega} i$$
 (25)

where $P^* = \begin{bmatrix} P_{ref} \\ Q_{ref} \end{bmatrix}$ and $R_{\omega} \in \mathbb{R}^{2 \times 2}$ is the weight matrix for control effort, $Q_{\omega} \in \mathbb{R}^{2 \times 2}$ represents the weight matrix for power tracking, and $G \in \mathbb{R}^{2 \times 2}$ denotes the voltage vector. The weighting matrices were chosen as $Q_{\omega} = diag(1,1)$ and $R_{\omega} = diag(0.01,0.01)$ to balance fast power tracking and reduced current stress.

Larger Q_{ω} improves accuracy, while higher R_{ω} smooths the current response. These values were found optimal through sensitivity analysis for stable and low-THD operation.

In order to calculate the P*, the active and reactive references are determined from the hybrid system PV-fuel cell system and the desired power factor as

$$P_{\text{ref}} = P_{\text{pv}} + P_{\text{fc}} \tag{26}$$

A fixed power factor and PV output are used to derive the reactive power reference:

$$Q_{\text{ref}} = \frac{P_{\text{ref}}}{PF_{\text{ref}}} \times \sqrt{1 - PF_{\text{ref}}^2}$$
 (27)

The optimal current reference vector is then obtained analytically as

$$\mathbf{i}^* = \begin{bmatrix} i_d^* \\ i_a^* \end{bmatrix} = -\mathbf{H}^{-1}\mathbf{f} \tag{28}$$

with the Hessian matrix H and the gradient vector f defined as

$$H = G^T Q_{\omega} G + R_{\omega} \tag{29}$$

$$f = -G^T Q_{\alpha} P^* \tag{30}$$

Substituting (29) and (30) into (28) yields the final closed-form solution.

$$\begin{bmatrix} i_d^* \\ i_a^* \end{bmatrix} = -(G^T Q_\omega G + R_\omega)^{-1} \cdot G^T Q_\omega \begin{bmatrix} P^* \\ O^* \end{bmatrix}$$
(31)

The advantages of this approach provide the optimal dq-axis current references in a single computational step, eliminating the need for iterative tuning and enabling faster dynamic response with improved robustness under varying operating conditions.

Also, it can be observed from the analytical expression of (31) that it yields a closed-form solution that requires only basic matrix algebra, which involves two matrix multiplications of size 2×2 , with an inversion of the computation performed in constant time. This enables the SQO controller to be highly efficient in real-time processing. Also, it can be observed that the optimal current vector i* will proportionally with slight variations in the system parameters (voltage values, impedance values), as the optimal current vector i* is proportional to the grid voltage matrix G and adaptive weight matrices Q_{ω} and R_{ω} . Hence, there is no need for online adjustments of the optimal current vector i*.

5. Results and discussion

The new quadratic optimization-based P-Q control operation for the PV-fuel cell hybrid gridtied system is verified under significant and sudden disturbances, as shown in Figs. 6-16. The irradiance profile results in sudden changes imposed on PV generation, with steps from $600 W/m^2$ to $1000 W/m^2$ and a sudden decrease to $500 W/m^2$. The hybrid control adapts by scaling down the fuel cell output P_{PF} in inverse proportion to PV power P_{PV} (Figure 7), keeping the total generation P_t constant and showing successful real-time power sharing between the two sources. The real power regulation profile (Figure 8) shows that the inverter power Pinv accurately tracks the reference Pref calculated by the quadratic optimization law in expression (31) with zero steady-state error and essentially zero overshoot, achieved without iterative PI gain adjustment, an important benefit of the proposed approach. Direct-axis current tracking (Figure 9) also confirms the accuracy of the active power loop, with id tracking i_d^* even under rapid setpoint change.

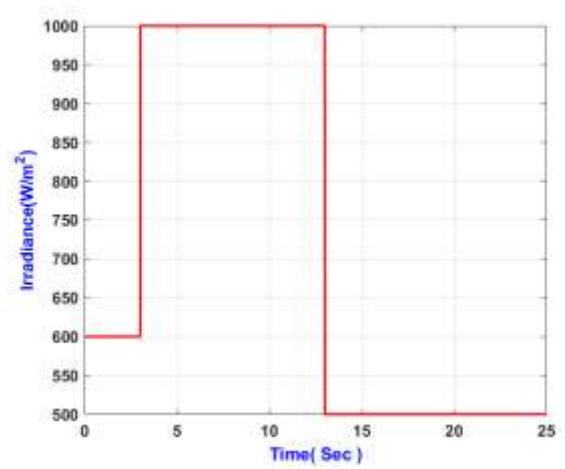


Figure 6. Irradiance profile.

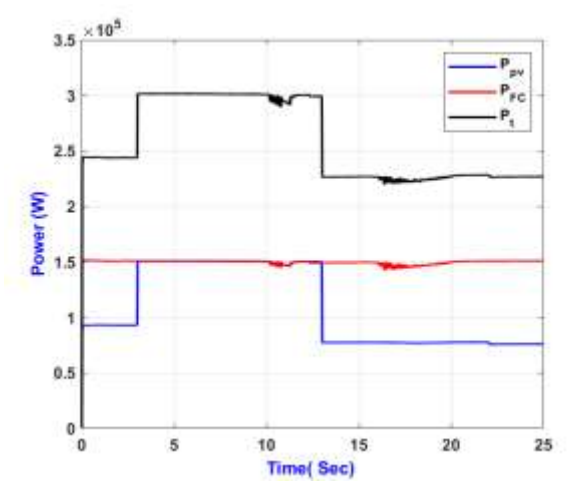


Figure 7. Power response of energy sources.

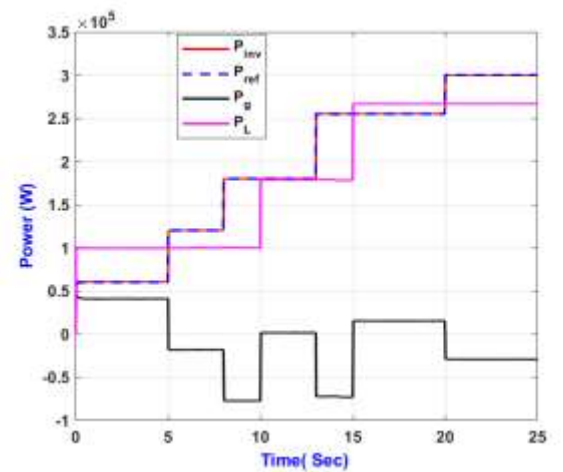


Figure 8. Real power regulation of a hybrid grid-tied system.

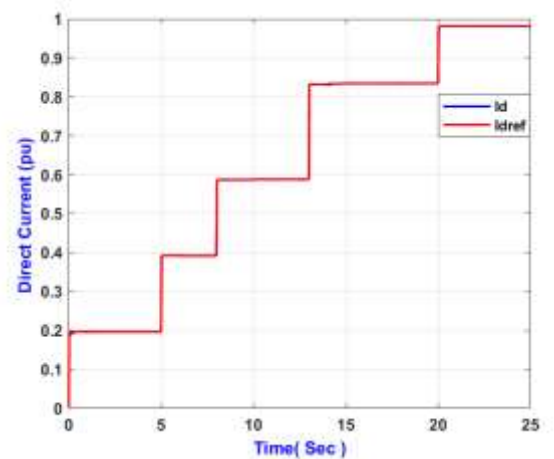


Figure 9. Id tracking response.

Reactive power control (Figure 10) demonstrates that Q_{inv} tracks Q_{ref} bidirectionally providing positive reactive power to support grid voltage when needed, or consuming negative reactive power to enhance power factor or regulate voltage levels. Quadrature-axis current tracking (Figure 11) is similarly precise, demonstrating that the reactive power loop enjoys the same rapid convergence and stability as the real power loop. Voltage waveforms for load, grid, and inverter (Figure 12) are maintained sinusoidal and synchronized, with figure 13 verifying accurate phase alignment between voltage and current, guaranteeing minimal reactive losses and effective power transfer. System frequency (Figure 14) is held tightly regulated at 50 Hz, with only minor, fleeting deviations during disturbances, verifying strong dynamic stability. Power factor (Figure 15) is maintained effectively unity throughout the simulation, a direct result of the accurate calculation of Q_{ref} and precise i_q tracking afforded by the quadratic optimization controller.

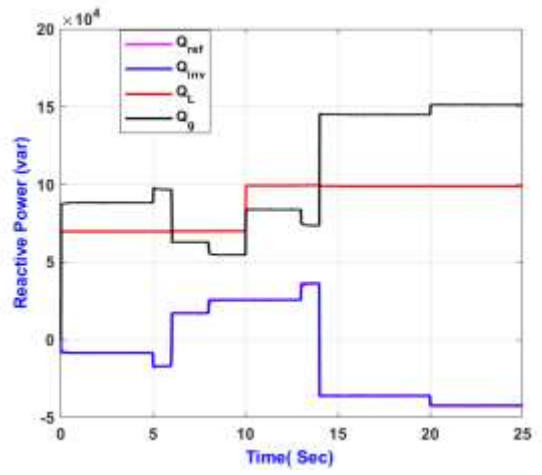


Figure 10. Reactive power regulation of a hybrid grid-tied system.

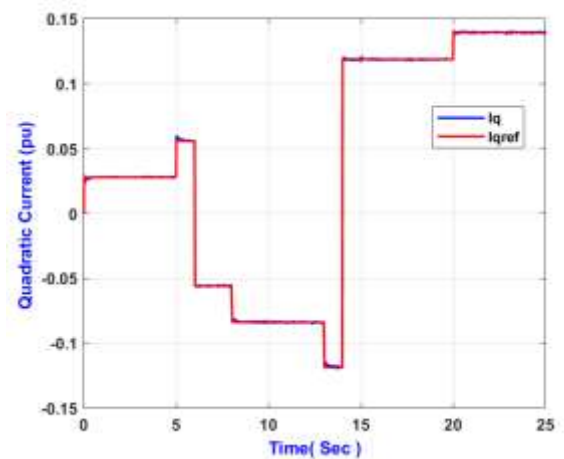


Figure 11. Iq tracking response.

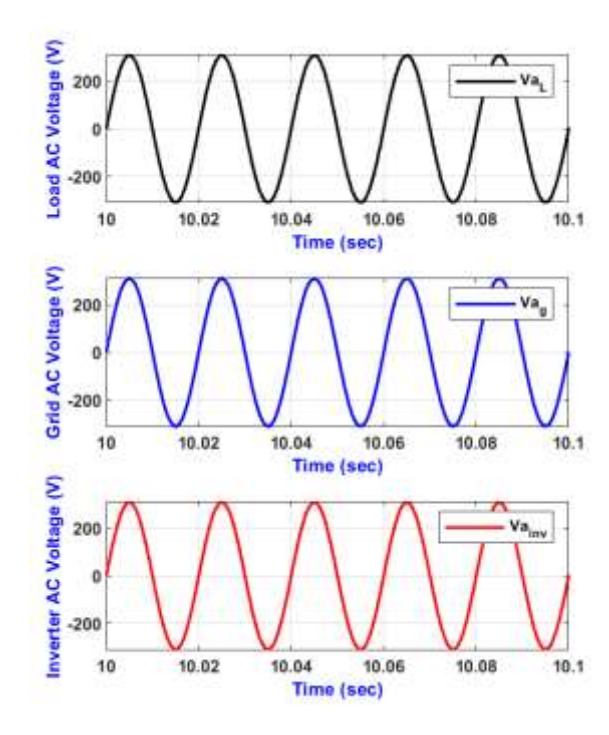
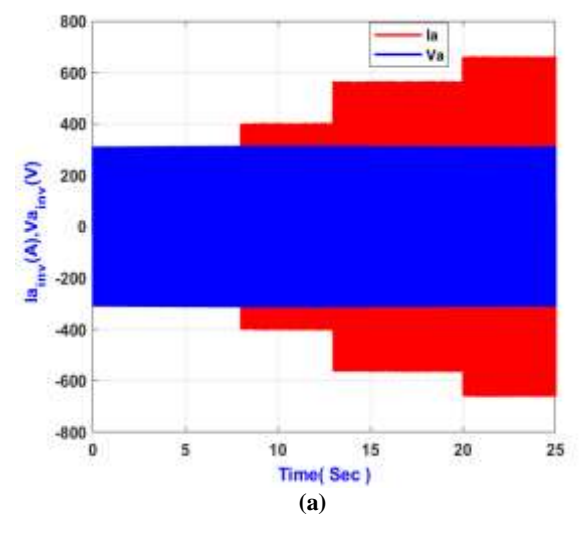
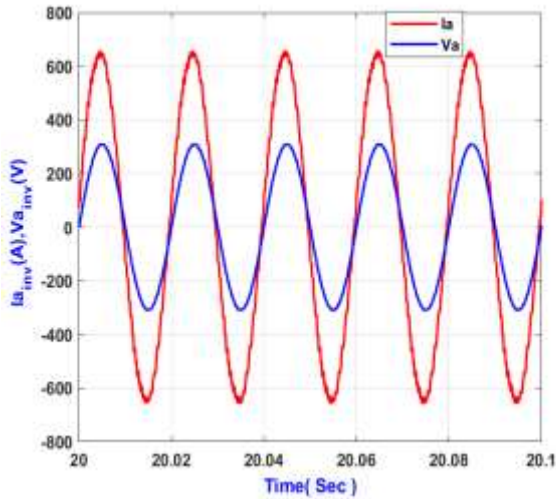


Figure 12. sine waveforms of load, grid and inverter.





(b)
Figure 13. (a) Phase voltage and current of the inverter,
(b) zoomed section.

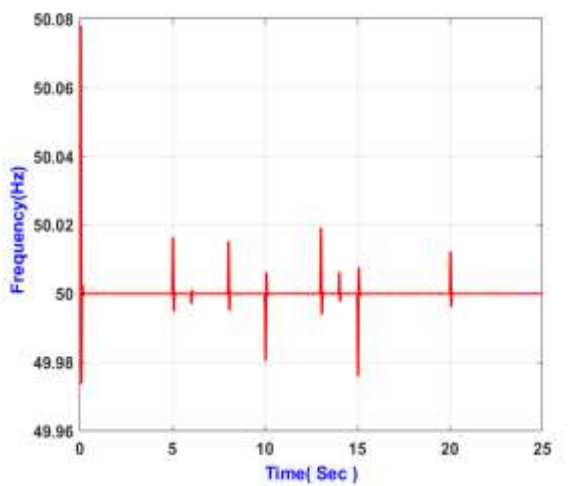


Figure 14. Frequency response of the system.

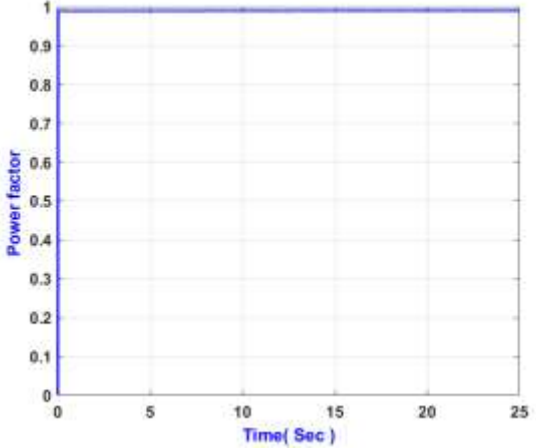
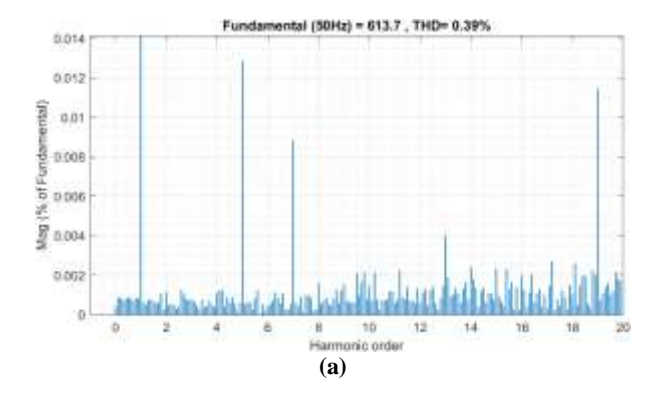


Figure 15. Power factor.

The outcomes of the harmonic analysis are depicted in figure 16. Figure 16 (a) shows the FFT of the inverter voltage, which exhibits a very low THD of 0.39%. This indicates an excellent level of voltage waveform quality in accordance with IEEE 519 guidelines. Figure 16 (b) shows the FFT of the inverter current with a THD of 1.20%. Thus, despite the current distortion, there is negligible distortion in the proposed SQO control strategy applied in this research. The results demonstrate that the current references calculated via mathematical computation successfully align the current vector with the grid voltage waveform while preventing unwanted switch transitions.

The results show that the proposed quadratic optimization controller achieves rapid transient response, high steady-state accuracy, and superior power quality over a broad operating range. It allows seamless PV-fuel cell coordination, accurate bidirectional reactive power control, unity power factor operation, and adherence to harmonic standards — all in a single-step computation that surpasses traditional PI-based approaches in both dynamic performance and robustness.



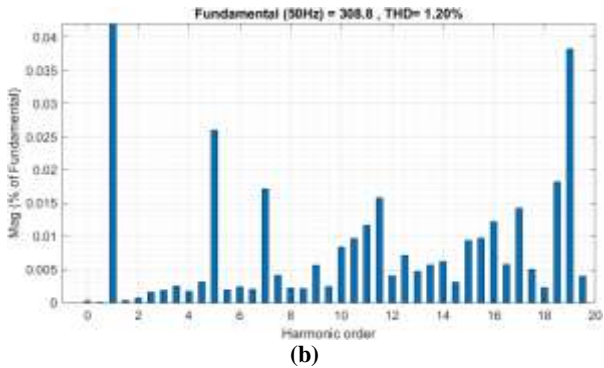


Figure 16. FFT spectrum analysis of harmonics for (a) inverter voltage, (b) inverter current.

In order to validate the proposed system, the quantitative metric steady-state values are calculated in table 4. As seen from table 4, all steady-state error deviations and RMS values of tracking error remain below 0.1% and 0.4 kVAr, respectively. Also, the settling time t_s (s) and the rise time t_r (s) All scenarios are calculated and indicate that the system is very fast-tracking with the reference values. This ensures near-perfect accuracy of the proposed SQO controller's tracking task.

Table 4: Quantitative steady-state error metrics.

Scenario	ΔP_{SS} %	ΔQ_{SS} %	RMS e _P kW	RMS e_Q kVA	t_s (s)	t_r (s)
Nominal PF=0.998	0.06	0.08	0.18	0.22	0.80	0.35
Irradiance step 600- 1000 $\frac{W}{m^2}$	0.08	0.11	0.24	0.31	0.92	0.41
Irradiance step 1000-500 W/m^2	0.09	0.12	0.27	0.34	0.95	0.44
Load step (+15%)	0.07	0.10	0.21	0.29	0.88	0.39

5. Performance comparison

For comparison consistency, all of the control methods, VOC [3], MPC [19], ANN [25], and the proposed SQO were evaluated using the same simulation parameters. The parameters selected include the same switching frequency of 20 kHz, DC-link voltage of 800 V, rated power of 300 kW, and filter values. This ensures that the difference in the simulation results of table 5 does not come from parameter differences. The performance indicators explored include power factor (PF), total harmonic distortion for inverter

current (THD_i), total harmonic distortion for inverter voltage (THD_v) , and the voltage and current phase shift ϑ_d), all obtained from simulated results. Referring to table 4, SQO demonstrates better performance compared to current baselines, achieving an optimal power factor of 0.998, a minimum total harmonic distortion for inverter current of 1.2%, for inverter voltage of 0.39%, and a minimum phase shift of only 0.12. These results confirm the effectiveness of SQO in achieving a near-unity power factor, better harmonic rejection, and voltage and current phase alignment, especially when compared to accepted standards such as VOC, MPC, and ANN under similar conditions in the hybrid photovoltaic-fuel cell system.

Table 5: Performance comparison of the proposed control with the state-of-the-art.

Reference	Control	PF	THDi	THD _v	ϑ_{d}
	approach		%	%	
[3]	VOC	0.953	2.82	1.04	0.72°
[19]	MPC	0.962	1.48	0.92	0.52°
[25]	ANN	0.958	1.75	0.63	0.64°
Proposed	SQO	0.998	1.2	0.39	0.12°

6. Conclusion

This paper proposed a SQO strategy for fast and accurate P-O control in a grid-connected PV-fuel cell system. The proposed analytical controller replaces conventional PI loops with a single-step quadratic cost optimization that directly computes the optimal dq-axis current references without iterative tuning. Using real-time grid voltage, current, and reference power measurements, the achieves fast dynamic response, controller accurate active and reactive power tracking, and robustness to sudden irradiance and load variations. Simulation results under realistic operating conditions verified a near unity PF (0.998), low. $THD_i=1.2\%$ and $THD_{ij}=0.39\%$, and stable operation within IEEE 519 limits. Compared with VOC, MPC, and ANN-based controls. the SQO approach consistently demonstrated superior tracking accuracy and phase alignment.

Future work will focus on hardware implementation and experimental testing under grid disturbances to validate the real-time performance and scalability of the proposed controller.

7. References

[1] Tiar, Mourad, et al. "Optimal energy control of a PV-fuel cell hybrid system." International Journal of Hydrogen Energy 42.2 (2017): 1456-1465.

- [2] Mirhassani, SeyedMohsen, et al. "Advances and challenges in grid tied photovoltaic systems." Renewable and Sustainable Energy Reviews 49 (2015): 121-131.
- [3] İnci, Mustafa. "Active/reactive energy control scheme for grid-connected fuel cell system with local inductive loads." Energy, vol. 197, pp. 117191, (2020).
- [4] Alsaidan, Ibrahim, et al. "An intelligent approach to active and reactive power control in a grid-connected solar photovoltaic system." Sustainability 13.8 (2021): 4219.
- [5] Saidi, Abdelaziz Salah. "Impact of grid-tied photovoltaic systems on voltage stability of tunisian distribution networks using dynamic reactive power control." Ain Shams Engineering Journal 13.2 (2022): 101537.
- [6] Andrade, Iván, et al. "An active/reactive power control strategy for renewable generation systems." Electronics 10.9 (2021): 1061.
- [7] Sunil Kumar, C., C. Puttamadappa, and Y. L. Chandrashekar. "Power quality improvement in grid integrated PV systems with SOA optimized active and reactive power control." Journal of Electrical Engineering & Technology 18.2 (2023): 735-750.
- [8] Ibrahim, Nagwa F., et al. "Comparative analysis of three-phase PV grid connected inverter current control schemes in unbalanced grid conditions." IEEE Access 11 (2023): 42204-42221.
- [9] Habib, Mustapha, et al. "Optimized management of reactive power reserves of transmission grid-connected photovoltaic plants driven by an IoT solution." International Journal of Electrical Power & Energy Systems 143 (2022): 108455.
- [10] S Pandey, Amarjeet, Manjunath Kallamadi, and Krupa Shah. "Cascaded AC–DC Voltage Control to Provide Reactive Power Support for the PV- Driven Grid- Tied Synchronverter." International Journal of Circuit Theory and Applications 53.6 (2025): 3778-3786.
- [11] Boopathi, Rajendran, and Vairavasundaram Indragandhi. "Enhancement of power quality in grid-connected systems using a predictive direct power controlled based PV-interfaced with multilevel inverter shunt active power filter." Scientific Reports 15.1 (2025): 7967.
- [12] Polat, Sezai, Emrah Biyik, and Hacer Şekerci Öztura. "Optimal active and reactive power scheduling for inverter-integrated PV and BESS under inverter current constraints." Electric Power Systems Research 245 (2025): 111629.
- [13] Elnaghi, Basem E., et al. "Experimental validation of an adaptive fuzzy logic controller for MPPT of grid connected PV system." Scientific Reports 15.1 (2025): 27173
- [14] Tsengenes, Georgios, and Georgios Adamidis. "Investigation of the behavior of a three phase grid-

- connected photovoltaic system to control active and reactive power." Electric Power Systems Research 81.1 (2011): 177-184.
- [15] Hamrouni, Nejib, Sami Younsi, and Moncef Jraidi. "A flexible active and reactive power control strategy of a LV grid connected PV system." Energy Procedia 162 (2019): 325-338.
- [16] Islam, Monirul, Nadia Afrin, and Saad Mekhilef. "Efficient single phase transformerless inverter for grid-tied PVG system with reactive power control." IEEE transactions on sustainable energy 7.3 (2016): 1205-1215.
- [17] Talha, Muhammad, S. R. S. Raihan, and N. Abd Rahim. "PV inverter with decoupled active and reactive power control to mitigate grid faults." Renewable Energy 162 (2020): 877-892.
- [18] Dhaneria, Asheesh. "Grid connected PV system with reactive power compensation for the grid." 2020 IEEE Power & Energy Society Innovative Smart Grid Technologies Conference (ISGT). IEEE, 2020.
- [19] Jain, Sarthak, Mohammad B. Shadmand, and Robert S. Balog. "Decoupled active and reactive power predictive control for PV applications using a grid-tied quasi-Z-source inverter." IEEE Journal of Emerging and Selected Topics in Power Electronics 6.4 (2018): 1769-1782.
- [20] Liu, Liming, et al. "Decoupled active and reactive power control for large-scale grid-connected photovoltaic systems using cascaded modular multilevel converters." IEEE Transactions on Power Electronics 30.1 (2014): 176-187.
- [21] Islam, Monirul, and S. Mekhilef. "A new high efficient transformerless inverter for single phase gridtied photovoltaic system with reactive power control." 2015 IEEE Applied Power Electronics Conference and Exposition (APEC). IEEE, 2015.
- [22] Sreekanth, Thamballa, Narasimhamurthy Lakshminarasamma, and Mahesh K. Mishra. "Grid tied single- stage inverter for low- voltage PV systems with reactive power control." IET Power Electronics 11.11 (2018): 1766-1773.
- [23] Muftah, Magdi G., et al. "A grid-tied PV-fuel cell multilevel inverter under PQ open-loop control scheme." Frontiers in Energy Research 10 (2022): 968371.
- [24] Albuquerque, Fabio L., et al. "Photovoltaic solar system connected to the electric power grid operating as active power generator and reactive power compensator." Solar Energy 84.7 (2010): 1310-1317.
- [25] Yilmaz, Unal, and Omer Turksoy. "Artificial intelligence based active and reactive power control method for single-phase grid connected hydrogen fuel cell systems." International Journal of Hydrogen Energy 48.21 (2023): 7866-7883.
- [26] Azab, Mohamed. "High performance decoupled active and reactive power control for three-phase grid-

- tied inverters using model predictive control." Protection and Control of Modern Power Systems 6.3 (2021): 1-19.
- [27] Alenius, Henrik, et al. "Autonomous reactive power support for smart photovoltaic inverter based on real-time grid-impedance measurements of a weak grid." Electric Power Systems Research 182 (2020): 106207.
- [28] Lodhi, Anuj, and Praveen Bansal. "Novel TDC-LMS Approach for Reactive Power Compensation in Fuel Cell-Based Smart Grids." Smart Grids and Sustainable Energy 10.3 (2025): 67.
- [29] Vendoti, Suresh, et al. "Grid tied hybrid PV fuel cell system with energy storage and ANFIS based MPPT for smart EV charging." Scientific Reports 15.1 (2025): 27392.
- [30] Aljohani, Mansour. "Enhancing the Performance of Grid-Tied Renewable Power Systems Using an Optimized PI Controller for STATCOM." International Journal of Robotics & Control Systems 5.2 (2025).
- [31] Patarroyo-Montenegro, Juan F., et al. "A linear quadratic regulator with optimal reference tracking for three-phase inverter-based islanded microgrids." IEEE Transactions on Power Electronics 36.6 (2020): 7112-7122